Omnidirectional source modeling for ray tracing in room acoustics with specular reflection

BENOIT BECKERS
Urban Physics Joint Laboratory
Université de Pau et des Pays de l'Adour
Allée du Parc Montaury, 64600 Anglet
FRANCE
benoit.beckers@univ-pau.fr, www.heliodon.net

Abstract: - The aim of this work is to show that the use of a ray tracing method based on stratified Monte Carlo with cells of equal area and equal aspect ratio gives the most convincing results in room acoustic simulation. It is compared with three other methods: the first one is very close but simply uses equal area cells, the second one is a Monte Carlo importance sampling and the last one is a standard Monte Carlo where the values of the spherical coordinates of the rays are generated randomly. These methods have similar complexity and comparable implementation. The experimentation is conducted in three steps: calculation of the sphere volume, exploration for reflections paths in a hexahedral enclosure, evaluation of standard acoustic parameters (Lateral Energy Fraction and Deutlichkeit). By starting from the volume of the sphere, the integration formula of sound rays contributions to a spherical receiver is derived in a transparent and purely geometric way.

Key-Words: - Ray tracing, Monte Carlo, room acoustics

1 Introduction

In the last third of the twentieth century, advances in computer technology have allowed a wide dissemination of ray tracing techniques, particularly in the areas of realistic rendering, lighting and acoustics [1]. The emergence of these techniques has accompanied the early development of CAD (Computer Aided Design) and computer graphics [2].

These methods are within the framework of the geometric optics and geometric acoustics [3]. [4] contains a formal proof of the equivalence of energy methods and ray tracing. Room acoustics deals with high frequency (typically in the band of 1000 Hz) in very large scenes (tens of meters in a concert hall, and even hundreds of meters in urban acoustics). Thanks to the progresses in numerical methods and the increasing power of computers, the application field of Finite Element Methods extends regularly, but as evidenced in [5], [6] and [7] among others, ray tracing methods remain significant. The history of this research field available in [8], an historical reference is given in [9] and the base of the present development is explained in [10].

This article proposes to introduce the discussion on the very particular problem of how to trace sound rays to simulate a perfectly omnidirectional point source, illustrating and evaluating the issues in the field of room acoustics more specifically associated to specular reflection.

In Section 2, the options for defining such a source are analyzed. Two deterministic and four random methods thus arise, involving the three families of Monte Carlo methods: standard Monte Carlo, importance sampling and stratified sampling.

In Section 3, these methods are tested and compared on a simple geometric problem: the calculation of the volume of the sphere. This calculation is completed by tracing rays from inside or outside sources. Section 4 assesses the ability of the methods in finding specular reflection paths in a very simple enclosure. Section 5 discusses the evaluation of two typical parameters of concert halls acoustics: Lateral Energy Fraction and Deutlichkeit.

2 Omnidirectional Source Simulation

In the standard Monte Carlo method, rays are traced from the center of a unit sphere and their directions (expressed by two angles in spherical coordinates: latitude and longitude) are randomly selected. This is equivalent to shoot randomly in the rectangle of the "plate carrée" projection of the sphere [11]. This method leads to a too high density of rays pointing toward the poles.

The best way to overcome this deficiency is to weight latitudes according to the distance of the points of the sphere to the plane of the equator. This is equivalent to shoot randomly in the rectangle of the equivalent cylindrical projection [12], also

called cylindrical equal area projection [11]. This method, which can be called importance sampling, is a v ariance reduction one. Such approaches are based on the observation that certain values taken by a random variable in a simulation have more effect than others on the desired estimator [13]. Both methods are summarized in Table 1.

In the stratified sampling Monte Carlo methods, rays' initial angles are selected not on the whole surface of the unity sphere, but inside cells whose union covers the sphere. The first step of these methods is therefore to mesh the sphere.

The action of creating a mesh will automatically provide the means to organize several deterministic ray tracings generated on the nodes or within the mesh, even if it is possible to generate uniformly distributed points on t he sphere without using meshes.

Table 1: Random calculation of the rays' directions

Pseudo code to define N random spherical coordinates on a hemisphere	
Random numbers	x = random $(N,1)$ y = random $(N,1)$
Generation of latitude α and longitude φ in standard Monte Carlo	$\alpha = x\,\pi\,/\,2$ $\varphi = y\,2\,\pi$
Generation of α and φ in importance sampled Monte Carlo	$\alpha = \arcsin(x)$; $\varphi = y\,2\,\pi$

On the basis of meridian arcs and parallel segments, built so as to have equal lengths, it is possible to generate sequences of points like in Fig.1a. Stenseng, quoted by [14], first defines the number of parallels on which the points will be distributed. Therefore, to obtain about 500 points, it is necessary to impose 14 parallels, giving 492 points, or 15 parallels, which would give 572 points. It is not possible to obtain an intermediate result.

To preserve the uniformity of the stratified Monte Carlo ray tracing, it is possible to impose cells of equal area. This led to various methods, including those based on regular polyhedrons, as in [15] and [16], but these approaches are limited by the fact that there are only five regular polyhedrons.

Other methods are based on a sphere meshing built on arcs of meridians and parallels. In the sky dome model [17], the design of the tiles is based on maximizing inscribed circles size in order to design scanners for sky luminance studies. In the proposed solution, the author reaches a very good coverage of the hemisphere by circles arranged along parallels. In [18], the mesh definition is based on the analogy with how to make igloos from almost identical snow bricks also arranged along parallels.

To build equal area cells, it is convenient to use the equal area projections of the sphere. The best known are the projection of Lambert [12] or the cylindrical one [19], whose 3D view is shown in Fig.1c, or the circular one [20], two 3D views of which are shown in Fig.1b and 1d. The last is the only one where the number of cells can be imposed exactly.

Looking at the two top domes in Fig.1, we note that Fig.1a has as many points as Fig.1b has cells, and it is clear that both have almost the same arrangement of points or cells.

The equal area (EA) meshes of Fig.1c and Fig.2a are congruent (except for the polar cell), while the two other meshes are not. For a nearly N cells mesh, we suggest to define the following n x m mesh, which exactly fills the hemisphere with a total number of cells: $N = nm + 1$ and ensures a very homogeneous distribution of elements:

$$n = \left\langle \sqrt{N/2} \right\rangle_{integer} \quad ; \quad m = \left\langle N/n \right\rangle_{integer} \qquad (1)$$

The mesh computed with (1) is systematically adopted in this publication when EA model is concerned. For 500 c ells required on t he hemispherical mesh, the found network is given by the relation: 33 x 15 + 1 = 496.
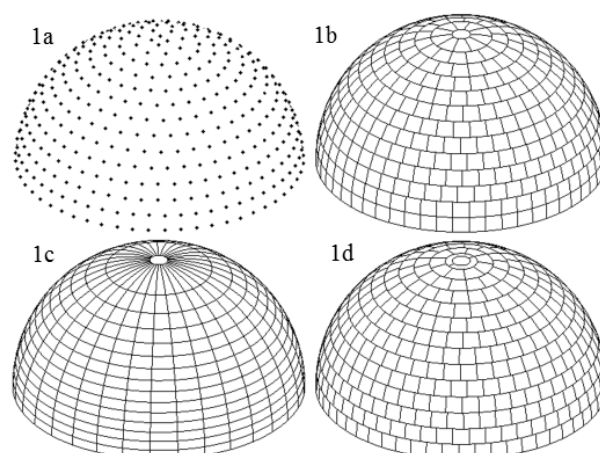

Fig.1 Four cells configurations: 1a and 1b: 492 points or cells, 1c and 1d: 496 cells

If congruence is not imposed, there is an additional degree of freedom to generate the mesh. We therefore propose to require that the aspect ratio of these cells on the sphere should be as close as possible to unity. For this reason, this kind of mesh is denoted EAR (equal aspect ratio).

This proposal was suggested by Tregenza [17], who sought to inscribe in each cell a circle with the maximum diameter. It has been developed in detail [20], by introducing a simple physical criterion: the covering index. This clearly shows that in the EA

model of Fig.1c, the aspect ratio is generally poor, except in the upper area of the circles 3 and 4 (Fig.3a). In the *EAR* model in Fig.1b and Fig.1d, the ratio is very good everywhere (Fig.3b). Note that, according to [21], the aspect ratio is optimal when the inscribed circles hit the four sides of their cells, which is the case in most of the cells in Fig.3b.
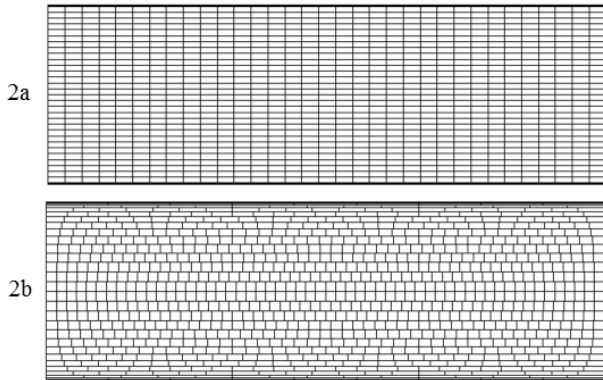

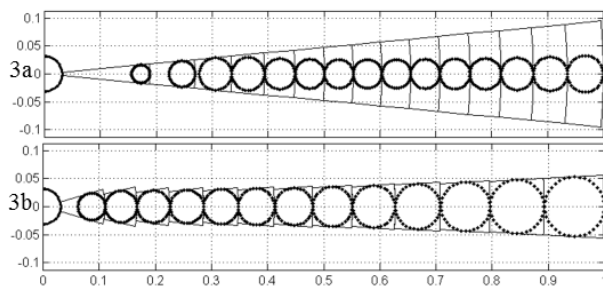Fig.2 Equal area Lambert cylindrical projections, 2a: 992 *EA* cells, 2b: 992 *EAR* cells

Fig.3 Coverage index = 0.25 for *EA* cells (3a) and 0.58 for *EAR* cells (3b)

3 Volume of the Sphere

3.1 Spherical pyramids
The first given example is that of evaluating the volume of a sphere. This example is representative of calculating not only convex solids, but also any volume, either in one piece or not. This procedure, which is not necessarily very effective, has the great advantage of calling only extremely simple geometric operators. These operators only need to be able to calculate the intersection of a line with a surface patch.

The volume of the sphere is calculated by adding the volumes of pyramids built on the spherical rays cast from the source located at any interior point. When tracing *N* rays in the unit sphere, if each of them corresponds to the same solid angle, it gives for the *N* spherical pyramids:

$$Sphere\ volume = \sum_{1}^{N} \frac{4\pi t^2}{N} \frac{t}{3} = \frac{4\pi}{3N} \sum_{1}^{N} t^3 \qquad (2)$$
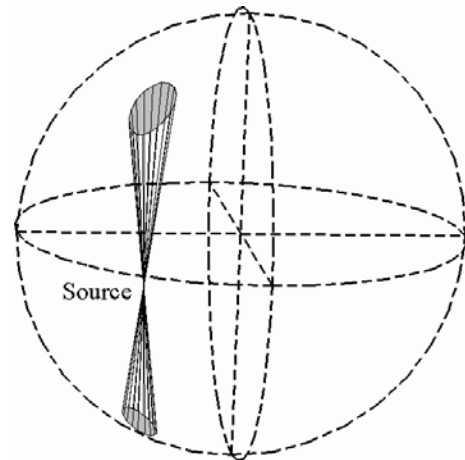

Fig.4 Spherical pyramids from an interior point, same solid angle and same axis

This process is shown in Fig.4, which shows two opposing cones that can be interpreted as pencils; they come from a p oint inside the sphere. The opening of the conical surface of Fig.4 is 1/20 steradian. The axis of the surface represents the two opposite rays traced from the source. The length of these rays is called *t*; for a uniform tracing of *N* rays, the base of each spherical pyramid is equal to $4\pi/N$ steradians. With an opening of 1/20 steradian, 80 π rays could cover the whole of the spherical surface, provided that there is no overlapping pencils.

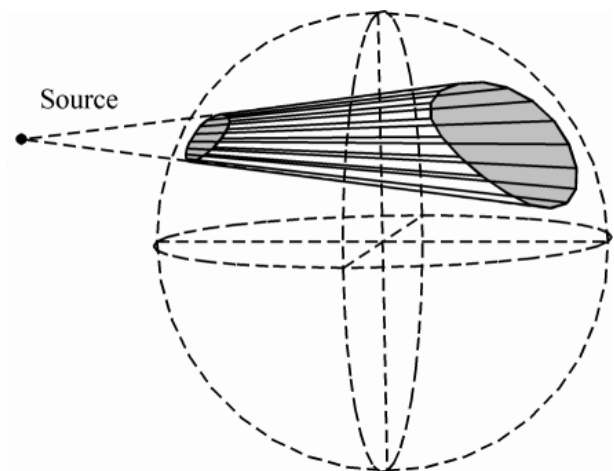Fig.5 Spherical pyramid built from an external point

When the source is located outside of the sphere (Fig.5), the solution is calculated according to the same principle as in (2), but, this time, a ray is taken into account only if it intersects the sphere twice. The solution is then obtained by calculating the difference between the two pyramids built on the ray. Of the *N* rays, n intersect the sphere twice, at

points located at distances t_i and t_o (with $t_o > t_i$) from the source. Therefore:

$$Sphere\ volume = \frac{4\pi}{3N} \sum_{1}^{n} \left(t_o^3 - t_i^3 \right) \quad (3)$$

The ray tracing methods are compared with each other in calculating the volume of the sphere by moving the source from the center to the outer surface. Regardless of the way followed to achieve the ray tracing, the result is equal to one when the source is at the center of the sphere. In the standard Monte Carlo, the result is rapidly deteriorating when the source moves away from the center of the sphere at a distance greater than one quarter of the radius, while in the importance sampling Monte Carlo, it remains remarkably stable regardless of the position of the source.

The poor result for the standard Monte Carlo method is due to the fact that the number of rays shot to the poles is much too high, resulting in significant bias regardless of the number of rays.

When tracing one million rays, as for the results listed in Table 2, the stratified Monte Carlo methods respectively give maximum errors of $2\ 10^{-4}$ % (*EA*) and $1\ 1\ 0^{-4}$ % (*EAR*), much lower than the error achieved in the importance sampling (*MC importance*).

To test less favorable conditions, we chose to compare the four methods with only 1000 rays (Table 3). As expected, the standard Monte Carlo (*MC standard*) gives poor results while the other three are very satisfactory, with less than 1% error for stratified methods.

Table 2: Comparison of Monte Carlo methods

Monte Carlo methods, 10^6 rays		
Distance to the center / radius	*MC standard* Error in %	*MC importance* Error in %
0	0	0
0.1	0.375	-0.04
0.2	1.494	-0.07
0.3	3.329	-0.10
0.4	5.829	-0.11
0.5	8.925	-0.10
0.6	12.516	-0.09
0.7	16.468	-0.06
0.8	20.596	-0.01
0.9	24.627	0.04
1.0	28.055	0.12

In conclusion, the stratified methods and the importance sampling method always give good results in this first test starting from an interior point of the sphere with, however, a net benefit to the stratified methods, and among these, a slight advantage for the *EAR* one. We observe the

hierarchy: *EAR*, *EA*, *MC importance* and *MC standard* in decreasing quality of the results.

Table 3: Comparison of the four Monte Carlo methods

Error in % for the Monte Carlo methods - 1000 rays				
(Distance to center)/radius	*MC standard*	*MC importance*	*E A*	*E AR*
0	0	0	0	0
0.1	0.46	-0.31	0.09	0.06
0.2	1.65	-0.55	0.19	0.12
0.3	3.51	-0.68	0.29	0.17
0.4	5.98	-0.68	0.39	0.22
0.5	8.95	-0.54	0.49	0.27
0.6	12.30	-0.21	0.59	0.32
0.7	15.89	0.32	0.69	0.38
0.8	19.48	1.07	0.79	0.43
0.9	22.80	2.07	0.88	0.49
1.0	25.30	3.37	0.99	0.56

3.2 Accuracy of the random method

To evaluate the performance of a Monte Carlo method, one carries out a number of tests under the same conditions and calculates the variance and standard deviation. Assuming that N tests produce a series of results x_i:

$$x_i\ ,\ i = 1\ , N \quad (4)$$

The average is calculated:

$$\overline{x} = \frac{1}{N} \sum_{i=1}^{N} x_i \quad (5)$$

The standard deviation is defined as:

$$\sqrt{\frac{1}{N} \sum_{i=1}^{N} \left(x_i - \overline{x} \right)^2} \quad (6)$$

For testing, graphs are built in different configurations. They show the value of the function, the average (thick broken line) and two continuous thick lines located above and below at a distance equal to the standard deviation. Fig.6 shows the evaluation of the sphere volume referred to the unit sphere one. An average of 1 and a very small standard deviation are expected. Although the source is located in an unfavorable position (right on the sphere surface), the solution is excellent in the case of the *EAR* method.

For all these simulations, as there is a stable value of the variance from about thirty trials, it was decided to perform systematically a minimum of fifty tests. For this experimentation, one hundred tests are performed. The relative mean volume is equal to 0.999 and its standard deviation to 0.0056.

With the same number of rays, the *EA* solution is a little worse (Fig.7); the standard deviation is 0.0076 instead of 0.0055. For the stratified Monte

Carlo with 100 trials and 1000 rays, the standard deviation is less than 1%, and a little better when cells of the same aspect ratio are used (Fig.6 and Fig.7).

The *MC importance* method gives similar results (Fig.8). The standard deviation is now equal to 0.0077, similar to the previous one.
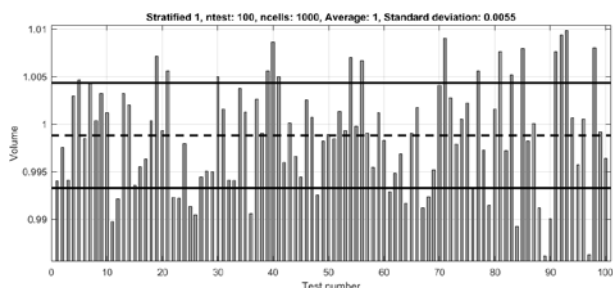

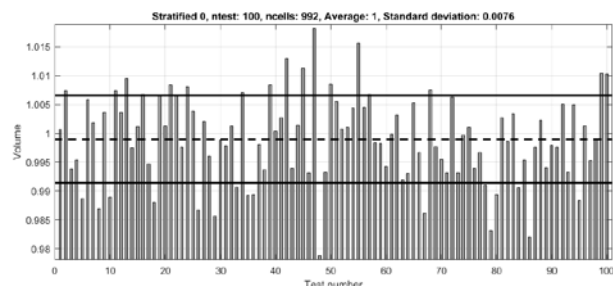Fig.6 Statistics for 100 tests of 1000 *EAR* cells
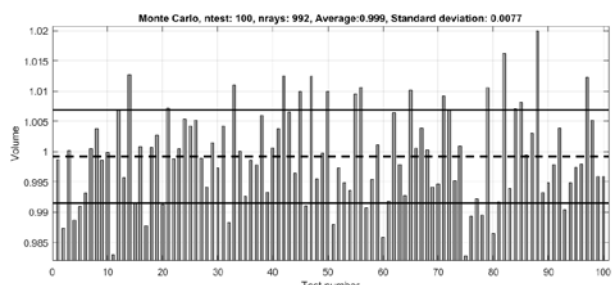

Fig.7 Statistics obtained in the 992 *EA* cells

Fig.8 Monte Carlo method based on importance sampling

3.3 Evaluation from an outside point

In the following sequence of tests, the volume of the unit sphere is calculated in several configurations obtained by moving the source from its center to a distance of five times the radius of the sphere. Two stratified sampling Monte Carlo methods are compared to their deterministic version based on the same mesh.

The *EAR* and *EA* methods are very close, but the first one is usually a little better than the second one (Table 4). It is interesting to note that in the comparison of the deterministic versions with 10000 rays, the *EA* method is better than the *EAR* one. This can be explained by a better configuration of *EA* cells in this particular case. But note that the

difference between the two solutions is minimal (0.3%), and that the random ray tracing corresponding to the same cells can give opposite results: 2.2% less for the *EAR* method.

Table 4: Deterministic and stratified *EAR* and *EA* cells

EAR and *EA* deterministic (det.) and stratified (strat.) Monte Carlo ray tracings. Gap in % between maximum and minimum found volumes for a source moving from its center to a distance of 5 radii			
N. rays	*EAR* (strat.)	*EAR* (det.)	*EA* (strat.)	*EA* (det.)
1000	12.9	17.3	20.1	21.1
10000	2.0	2.6	4.2	2.3
100000	0.4	0.2	0.6	0.3
10^6	0.053	0.015	0.058	0.028

In this example, for calculating the volume, ray trace becomes less effective from the outside than from the inside of the sphere. Gradually, as the distance grows, only the rays included in the cone encompassing the sphere contribute to the calculation of the volume. But this configuration is highly interesting, because it anticipates the typical case where a sound field is evaluated on a spherical receiver, as in the following sections of this paper.
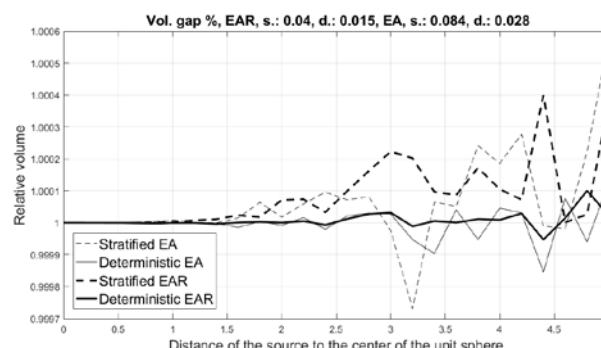
Fig.9 Sphere volume obtained with deterministic and stratified sampled methods (10^6 cells)

All simulations of Table 4 have the same characteristic: the accuracy is very good up to the distance of 1, which corresponds to the surface of the sphere, and then it slowly deteriorates when it moves away. The test with one million rays is shown in Fig.9. The error is always less than half a thousandth of the volume. For the stratified and deterministic *EAR* cases, we obtain gaps between maximum and minimum value equal respectively to .04 % and .015 %. For the *EA* case, we have 0.084 % and 0.028 %.

4 Searching the Number of Reflection Paths

As stated in the introduction, many conventional applications of ray tracing, once considered obsolete because needing very long calculation times, again become accessible today thanks to the evolution of graphics cards. The paths method [22] seems to be part of this renewal, for real-time applications in the field of entertainment where one tries to obtain, in a very short time, a d iscrete echogram. When the method of images is unsuitable because of the complex geometry of the scene, this method provides an interesting alternative [23], as it can benefit from advanced techniques implemented in realistic rendering.

In this study, we investigate the largest possible number of paths linking the source to the receiver by tracing a limited number of rays. A path is defined by the sequence of walls on which the ray is reflected. The purpose of this research based on the image's theory is to reconstruct valid paths [24, 25]. Once identified, the paths can be used to define the echograms as in the method of images.

The tests are performed on a t rapezoidal enclosure (Fig.10) defined by 6 normal vectors connecting the origin to the faces; In Matlab notation [-2 -1 0; 0 -2 0; 4 -1 0; 0 10 0; 0 0 -2.5; 0 0 2.5]. In the same figure, the source and the receiver are located at both ends of the thick line. The source is located at the origin of coordinates and the spherical receptor in [1 .2 7]. The radius of the receiver is calculated by the formula, [26]:

$$r = \left(\frac{15V}{2\pi N} \right)^{1/3} \tag{7}$$

In this formula, V is the volume of the enclosure and N the number of traced rays. For the analyzed case, we obtain the radius r = 1.12 which is rounded to 1.
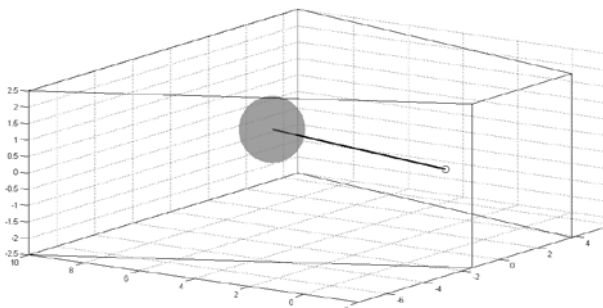

Fig.10 Trapezoidal enclosure used for paths detection

The process involves casting rays in all directions from the source. The rays are reflected on the walls of the enclosure and in sometimes intersect the spherical receiver. In these cases, we examine the route, that is to say, the sequence of walls on which the reflections have occurred. If the path is new, it is stored and the examination of the ray is continued.

The statistics of the results obtained in 50 tests are summarized in Table 5. The numbers separated by a d ash represent the number of detected reflections (or possible images) and the number of tests in which this number has been found.

The even columns show the proportion of cases lying in each category 40-50, 50-60, …,110-120.

In the last row of the table, we observe that the mean number of segments is increasing from 62 for the standard Monte Carlo to 94 f or the stratified Monte Carlo based on *EAR* cells.

The *EAR* stratified Monte Carlo method clearly shows its superiority over the others, even for a relatively small number of rays: 1000 in this case. Other tests were also made with less rays, but, on the one hand, they require a disproportionately large receiver radius and, on the other hand, the results are fairly unstable. In all the tests, the hierarchy of the methods of Table 5 is met: in descending order: *EAR*, *EA*, *MC importance* and *MC standard* This outcome corresponds to the inference previously attained in the calculation of the volume of the sphere.

5 Acoustical Parameters in Enclosure

To address the definitions of acoustic parameters, the sound intensity is evaluated in the ray tracing method. Going back to the formula (3), which gives the volume of a sphere, the development is performed as follows. Let note that the parameter t represents the distance from the source to the receiver surface. This parameter t is assimilated to the distance R from the source to the center of the receiver. V_r is its volume, N is the number of rays and n is the number of rays reaching the receptor.

$$V_r = \frac{4\pi}{3N} \sum_1^n \left(t_o^3 - t_i^3 \right)$$
$$= \frac{4\pi}{3N} \sum_1^n \left(t_o - t_i \right) \left(t_o^2 + t_o t_i + t_i^2 \right)$$
(8)

By assimilating the sum of the second-degree terms to $3R^2$, we get:

$$t_o^2 + t_o t_i + t_i^2 = 3R^2 \qquad (9)$$

By replacing $t_o - t_i$ by s, which is the length of the secant of the receiving sphere:

$$V_r = \frac{4\pi}{3N}\sum_1^n s \ \ 3R^2 \qquad (10)$$

Table 5: Number of paths detected with four Monte Carlo methods (50 tests, 1000 rays, 5 reflections)

Number of detected paths							
Standard MC		**Imp. MC**		**Stratified MC EA**		**Stratified MC EAR**	
	%		%		%		%
49-1	**2**						
51-1 53-5 54-1 57-2 58-4 59-5	**36**						
60-1 61-1 62-5 63-2 64-4 65-4 66-4 67-2 69-1	**48**	64-2 66-2 67-1 68-1 69-2	**16**				
70-1 71-1 72-1 73-1 74-1 75-1 77-1	**14**	70-8 72-4 73-3 74-5 75-2 76-4 77-3 78-2 79-6	**74**	72-1 73-1 74-2 78-2 79-2	**16**	75-1 77-1	**4**
		81-1 82-1 84-1 87-2	**10**	80-2 81-2 83-1 84-1 85-1 86-4 87-2 88-3 89-2	**36**	83-1 85-4 86-2 87-4 88-1 89-3	**30**
				90-2 91-5 92-1 93-1 94-3 95-2 97-1 98-1 99-1	**34**	90-2 91-2 92-2 93-2 94-2 95-5 96-1 97-4 98-1 99-1	**44**
				100-1 101-2 102-1 105-1 107-1	**12**	100-1 102-5 103-1 104-1 107-1	**18**
				111-1	**2**	112-1 114-1	**4**
Aver.: **2**		Aver.: **74**		Average: **89**		Average: **94**	

Replacing the sum of the secants by their average:

$$n\,\bar{s} = \sum_1^n s \qquad (1)$$

We deduce from (10):

$$\frac{1}{R^2} = \frac{4\pi n\bar{s}}{NV_r} = \frac{n}{N}\frac{4\pi\bar{s}}{V_r} \qquad (2)$$

And so, with I, the intensity (Wm^{-2}) and P the source power (W):

$$\frac{I}{P} = \frac{1}{4\pi R^2} = \frac{n}{N}\frac{\bar{s}}{V_r} \qquad (13)$$

At the distance R from the source, for a spherical receiver of radius r, sound intensity depends on the source power P and the ratio n of the rays that intersect the receiving sphere to the total number of traced rays. It also depends on the weight coefficient $\bar{s}$ of dimension (m^{-2}) which is the ratio of the mean length of the secants and the volume of the spherical receiver.

In practice, the sound level is expressed in decibels (*dB*):

$$10\log_{10}\left(10^{12} I\right) = 120 + 10\log_{10} I$$
$$10\log_{10}\left(10^{12} P\frac{n}{N}\frac{3\bar{s}}{4\pi r^3}\right) = 120 + 10\log_{10}\left(P\frac{n}{N}\frac{3\bar{s}}{4\pi r^3}\right) \qquad (14)$$

These developments do not take into account the time variable. Everything occurs as if the ray propagation was instantaneous. However, in acoustics, it is far from being the case. In the ray method, it is possible to reintroduce the time by taking into account the lengths of the rays, which is equivalent to sort them by time intervals.

After introducing the time variable, the definitions of acoustic parameters can be addressed. Barron [27] defines the lateral energy fraction *LF* ("Lateral energy fraction") which involves time

integrated intensities, for example E_0^{50}, which is the integral of the intensity between 0 a nd 50 milliseconds. They are energy densities, therefore expressed in Joule m^{-2}. The lateral energy fraction is an adimensional number smaller than one.

$$LF = \frac{\int_0^{80} p_{lat}^2(t)\,dt}{\int_0^{\infty} p^2(t)\,dt} = \frac{[E_{lat}]_0^{80}}{E_0^{\infty}}$$

(15)

This function is taking into account the angle of the ray arriving on the receptor and the direct one. The energy is weighted with the sinus of the projection of this angle in the horizontal plane allowing the rendering of the laterality effect.

Another acoustic parameter called clarity was introduced in [28] under the name of "Deutlichkeit". It is the ratio between the early energy (up to 50 milliseconds) and the total one. It is also an adimensional number smaller than one [29, 30].

$$D = \frac{\int_0^{50} p^2(t)\,dt}{\int_0^{\infty} p^2(t)\,dt} = \frac{E_0^{50}}{E_0^{\infty}}$$

(16)

A first test is performed to observe the behavior of these parameters wherein the number of reflections is varied. In the enclosure of Fig.10, we cast 10000 rays on a r eceiver with radius equal to 0.5. All the walls have the same absorption coefficient equal to 0.5 and the *EAR* deterministic method is used.

The global sound level increases with the number of reflections and approaches 70 *dB* (Table 6). The *LF* becomes quite constant just under 32% and the Deutlichkeit under 86%. This level has already been reached for 6 reflections.

Table 6: Acoustic parameters performance

Number of reflections	Global level *dB*	*LF* %	Deutlichkeit %
1	66	16.8	100
2	68	24.3	99.6
3	69	28.4	96.8
4	70	30.6	92.9
5	70	31.6	88.9
6	70	31.9	86.8
7	70	32.0	85.9
8	70	31.8	85.5
9	70	31.8	85.3
10	70	31.7	85.2
…			
20	70	31.7	85.0

The direct sound exact solution is given in watts by the formula (13) or in decibels by:

$$L_p = 10\left[\log(10^{12} P) - \log R^2\right] - 11$$

(17)

In this formula, *P* is the power of the source and *R* the distance from the source to the receiver (both are presumed point-wise). It is easy to verify that, if *P* = 0.001, the first term of the formula is equal to 90 *dB*. For *R* = 10 meters, L_p = 59 *dB*. In the concerned enclosure, it is 62 *dB*. The delay is equal to 20 m illiseconds. In all the 10,000 ray tests, the direct sound level is identical to its theoretical value.

The experiment follows with tests based on 10,000 cells. The reflection coefficient is equal to 0.5 and the number of reflections limited to 6. The sound levels are calculated in *dB* according to (14) which refers to a spherical receiver.

In the tests carried out to characterize the methods of ray tracing, it turned out that the number of rays was very important, but not the number of tests. In fact, from 20 trials, a good stability of the results is obtained.

In all the conducted tests, the usual hierarchy of methods is observed with respect to the standard deviation. We always see in Table 7 corresponding to tests involving 6 r eflections and an absorption coefficient equal to 0.5, an increasing standard deviation when following the same sequence as before: *EAR*, *EA*, *MC importance* and *MC standard*.

Table 7: *LF* & Deutlichkeit

Method 10000 rays, 20 tests	*LF*		Deutlichkeit	
	Av. (%)	*SD* (%)	Av. (%)	*SD (%)*
EAR	32.84	0.25	86.2	0.40
EA	32.87	0.97	86.2	0.47
MC importance	31.74	2.22	86.2	1.28
MC standard	31.46	2.42	85.9	1.47

4 Conclusion and Perspectives

As a r esult of the performed tests, the main conclusion is that one should always use the Monte Carlo stratified method based on cells of the same aspect ratio (*EAR*). This method always gives the best results in purely geometric tests such as sphere volume assessments using an internal or external source. It is also the most efficient in the search for reflection paths (approach used to recover images). Finally, in the case of acoustic parameters, it is more competitive than the other ones. It is as easy to

implement as any other and preserves the control of the number of cast rays.

These features make it a perfect candidate for the solution of acoustic simulations of real time problems that require fast response time and therefore the smallest possible number of rays [23].

The calculation of the volumes presented in the first part of the article not only allowed to classify methods in purely geometrical problems, but it also led to an elegant interpretation of the calculation of sound level based on the lengths of the secants of the receiver.

The proposed meshes can provide the basis of developments in tracing pyramids as suggested in [19]. In these problems, we should replace the tiles based on meridians and parallels with tiles based on meridians and great circles. The optimized formulation *EA* as described in § 2 c an easily adapt to these situations since they are based on congruent meshes with equal areas (*EA*). Note that when the *EA* method is as well conditioned as here, it gives almost as good results as the *EAR* method.

The last point to emphasize is that this new ray tracing method is likely to significantly improve the performance of algorithms making simultaneous uses of diffuse and specular reflection [31]. Indeed, for the diffuse reflection, as ray tracing is performed at several levels (actually, each reflection), the advantage of the *EAR* method has a multiplicative effect.

References:
[1] Appel A., Some techniques for shading machine renderings of solids, *AFIPS Conference Proc.* 32 1968, pp.37 - 45.
[2] Sutherland I.V., Sproull R.F., Schumaker R.A., A characterization of Ten Hidden-Surface Algoritmms, *Computing Surveys*, Vol. 6, No 1, March 1974, 55 pages.
[3] Kulowski A., Algorithmic Representation of the Ray Tracing Technique, *Applied Acoustics* 18 (1985), pp 449 - 469.
[4] Le Bot A., Bocquillet A., Comparison of an integral equation on energy and the ray-tracing technique in room acoustics, *J. Acoust. Soc. Am.* 108 (4) October 2000, pp 1732 - 1740.
[5] Harari I., A survey of finite element methods for time-harmonic acoustics, *Comput. Methods Appl. Mech. Engrg*. 195 (2006), pp 1594 - 1607.
[6] Łodygowski T., Sumelka W., "Limitations in application of finite element method in acoustic numerical simulation", *J. Theor App Mech* 44, 4 Warsaw 2006, pp 849 - 865.

[7] Thompson L.L., A review of finite-element methods for time-harmonic acoustics, *J. Acoust. Soc. Am.* 119 (3), March 2006, pp 1315-1330.
[8] Svensson P., The Early History of Ray Tracing in Room Acoustics, in *Reflections of sound*, Edited by Peter Svenson, NTNU, Norwegian University of Science and Technology, 2008, pp 37 - 48.
[9] Beckers B., Borgia N., The Acoustic Model of the Greek Theatre, *Protection of Historical Buildings - PROHITECH* 2009, Roma, Italy, June 21 - 24 2009.
[10] Beckers B., Calcul par la méthode des images de la réflexion spéculaire dans des enceintes prismatiques convexes, *Report Acou 003*, http://heliodon.net/, 2017.
[11] Beckers B., Beckers P., *Reconciliation of Geometry and Perception in Radiation Physics*, FOCUS Series in Numerical Methods in Engineering, Wiley-ISTE, July 2014, 192 pages.
[12] Lambert J.H., *Photometria sive de mensura et gradibus luminis, colorum et umbrae*, Augsburg, C. Detleffsen for the widow of Eberhard Klett, 1760.
[13] Tokdar S.T., Kas R.E., Importance Sampling: A review, *WIREs Comp. Stat* 2010, 2, pp 54 – 60.
[14] Krokstad A., Strom S., Sorsdal S., Calculating the acoustical room response by the use of a ray tracing technique, *Journal of Sound and Vibration,* 8 (1968), pp 118 - 125.
[15] Randall, D.A., Ringler, T.D., Heikes, R.P., Jones, P and Baumgardner J., Climate modeling with spherical geodesic grids, *Computing in Science & Engineering* , Volume 4, Issue 5, Sept.-Oct. 2002 pp 32 – 41.
[16] Gregory M.J., Kimerling A.J., White D., Sahr K., A comparison of intercell metrics on discrete global grid systems, *Computers, Environment and Urban Systems* 32 (2008) pp 188 – 203.
[17] Tregenza PR., Subdivision of the sky hemisphere for luminance measurements, *Lighting Research & Technology*; 19 1987, pp 13 – 14.
[18] Crittenden R. G., Igloo Pixelizations of the Sky, *Astro. Lett. and Communications*, Vol. 37 2000, pp 377 - 382.
[19] Farina A., Pyramid Tracing vs. Ray Tracing for the Simulation of Sound Propagation in Large Rooms, in COMACO95, *Proc. of Int. Conf. on Computational Acoustics and its Environmental Applications*, Southampton,

England, Comp. Mechanics Publ., Southampton 1995, pp 1 - 9.

[20] Beckers B., Beckers P., A general rule for disk and hemisphere partition into equal area cells, *Computational Geometry*, vol. 45 no. 7 2012, pp 275 - 283.

[21] Beckers B., Beckers P., Sky vault partition for computing daylight availability and shortwave energy budget on a n urban scale, *Lighting Research & Technology*, 46 December 2014 pp 716 - 728.

[22] Tsingos N., Carlbom I., Elko G., Funkhouser T., Kubli R., Validation of Acoustical Simulations in the "Bell Labs Box", *IEEE Computer Graphics and Applications*, 2002, 22 (4), pp 28-37.

[23] Gu C., Zhu M., Lu H., Beckers B., Room impulse response simulation based on e qual-area ray tracing, *Audio Language and Image Processing International Conference (ICALIP)*, 2014, Shanghai, China, pp 832 – 836.

[24] Borish J., Extension of the image model to arbitrary polyhedra, *J. Acoust. Soc. Am.,* Vol 75, No.6, June 1984, pp 1827 – 1836.

[25] Lehnert H., Systematic Errors of the Ray-Tracing Algorithm, *Applied Acoustics 38* (1993) pp 207 - 221.

[26] Zeng X., Chen K., Sun J., On the accuracy of the ray-tracing algorithms based on various sound receiver models, *Applied Acoustics* 64 (2003) pp 433 - 441.

[27] Barron M., The subjective effects of first reflections in concert halls - The need for lateral reflections, *Journal of Sound and Vibration* 15(4) 1971, pp 475 - 494.

[28] Thiele R., Richtungsverteilungs und Z eitfolge der Schallruckewurfe in Raumen, *Acustica* 3, 1953, pp 291 – 302.

[29] Bradley J.S., The evolution of newer auditorium acoustics measures, *Canadian Acoustics / Acoustique Canadienne* 18 4 1990, pp 13 - 23.

[30] Fazenda B., Romero-Perez J., 3-dimensional room impulse response measurements in critical listening spaces, *Proceedings of the Institute of Acoustics*, 30 (6), (2009), pp 232 – 239.

[31] Lewers T., A combined Beam Tracing and Radiant Exchange computer model of room acoustics, *Applied Acoustics,* Vol. 38 no.s 2-4 (1993), pp 161 - 178.